# Reconciling Sensitivity and Breathability in Flexible Iontronic Pressure Sensors via Hierarchical Fibrous Architecture

Qi Zhang[1,2], Zidong He[1,2]*, Fali Li[2], Qianghu Zhu[2], Yaoping Yu[1], Boquan Zhao[2], Yuanzhao Wu[1,2]*, Min Tang[1], Kun Wei[1], Jie Li[1], Yiwei Liu[1,2], Haoyu Wang[1]*

[1] Innovation Center for Flexible Wearable Technology in Smart Rehabilitation Medicine, Ningbo Rehabilitation Hospital, Ningbo, Zhejiang 315040, China

[2] Zhejiang Key Laboratory of Magnetic Materials and Applications, Ningbo Institute of Materials Technology and Engineering, Chinese Academy of Sciences, Ningbo, Zhejiang 315201, China

Corresponding author: Zidong He, Yuanzhao Wu, Haoyu Wang

E-mail: hezidong@nimte.ac.cn (Dr. Z. D. He); wuyz@nimte.ac.cn (Prof. Y. Z. Wu); 13857833875@139.com (Dr. H. Y. Wang)

Keywords: flexible pressure sensors, iontronic, electrospinning, hierarchical architecture, wearable physiological monitoring

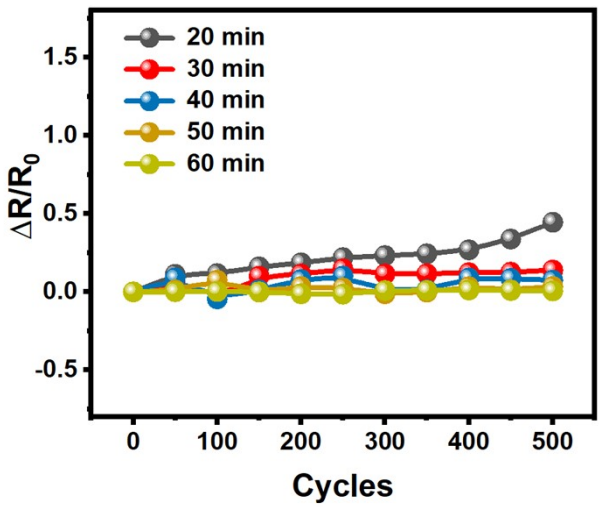


Fig. S1. Relative resistance variation of fibrous fabric electrodes with different MA electrospinning times over 500 bending cycles.

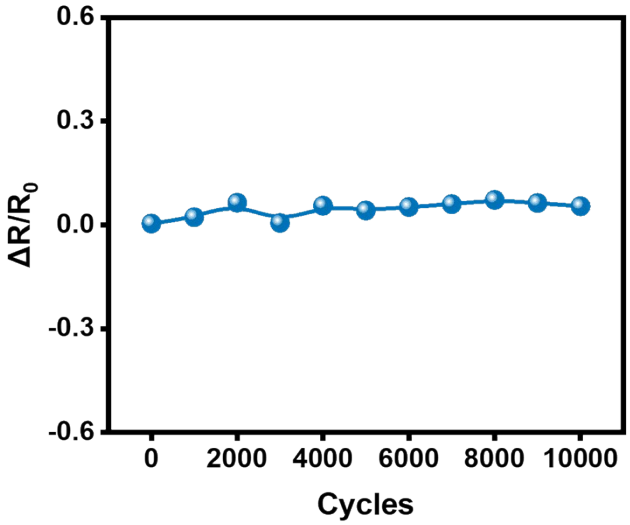


Fig. S2. Relative resistance variation of P(VDF-HFP)/MA/AgNWs fibrous fabric electrodes after 10000 bending cycles.

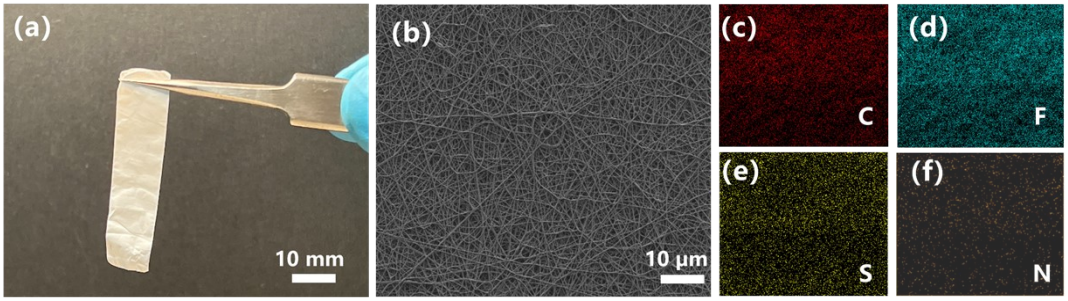


Fig. S3. (a) Photograph of the ionic nanofibrous membrane; (b–f) scanning electron microscopy (SEM) images and corresponding energy-dispersive X-ray spectroscopy (EDS) elemental mapping of the ionic nanofibrous membrane.

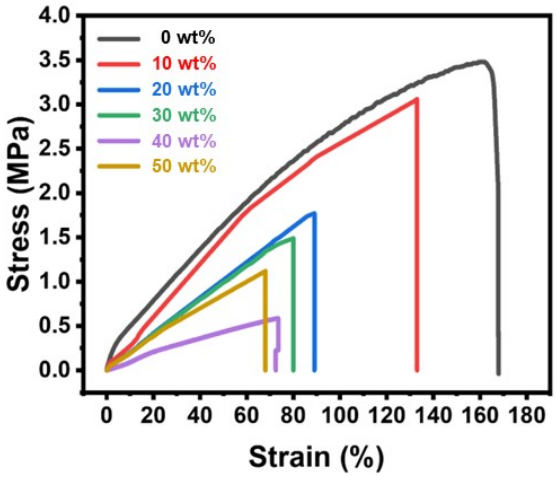


Fig. S4. Stress–strain curves of fibrous membranes with different ionic liquid contents.

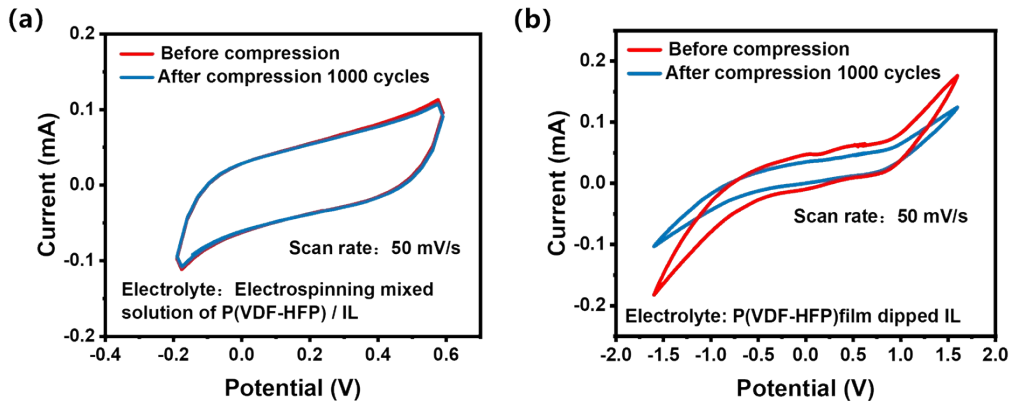


Fig. S5. Electrochemical CV curves of (a) co-electrospun P(VDF-HFP)/IL nanofibrous membranes and (b) IL-impregnated P(VDF-HFP) fibrous membranes before and after 1000 compression cycles at 5 kPa.

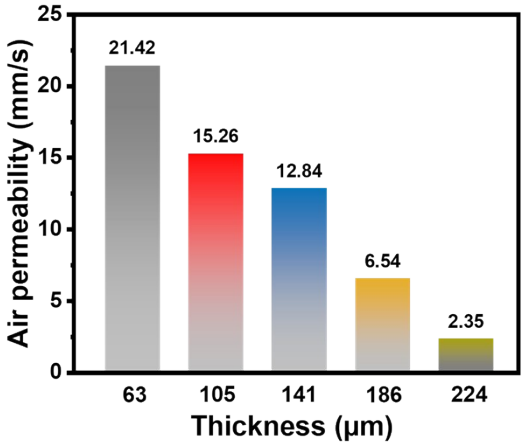


Fig. S6. Comparison of air permeability among pressure sensors incorporating ionic membranes of different thicknesses.

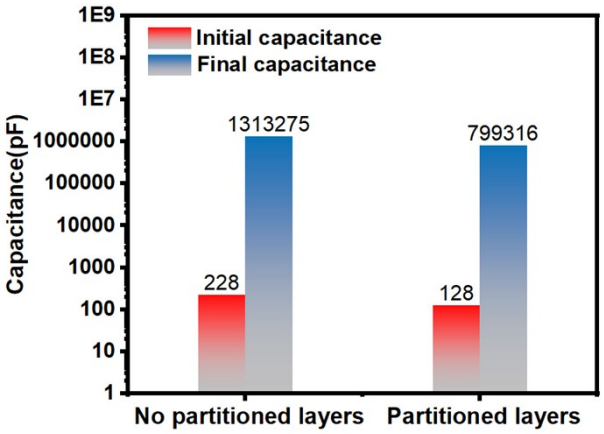


Fig. S7. Initial capacitance (at 0 kPa) and final capacitance (at 200 kPa) of sensors with and without the fibrous separator.

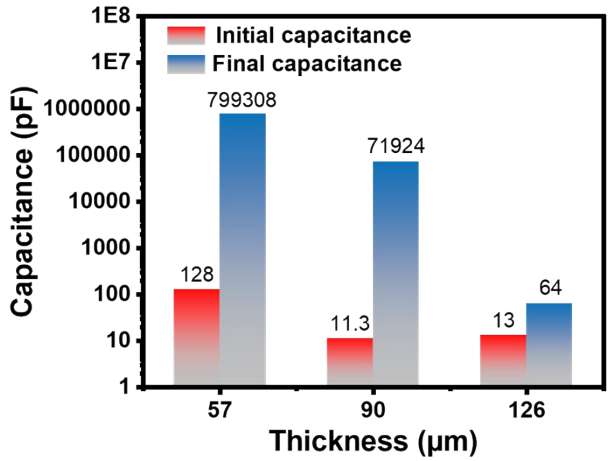


Fig. S8. Initial capacitance (at 0 kPa) and final capacitance (at 200 kPa) of pressure sensors with separators of different thicknesses.

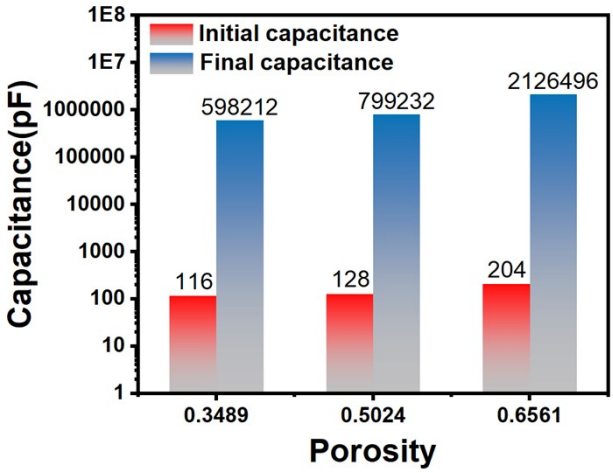


Fig. S9. Initial capacitance (at 0 kPa) and final capacitance (at 200 kPa) of pressure sensors with separators of different porosities.

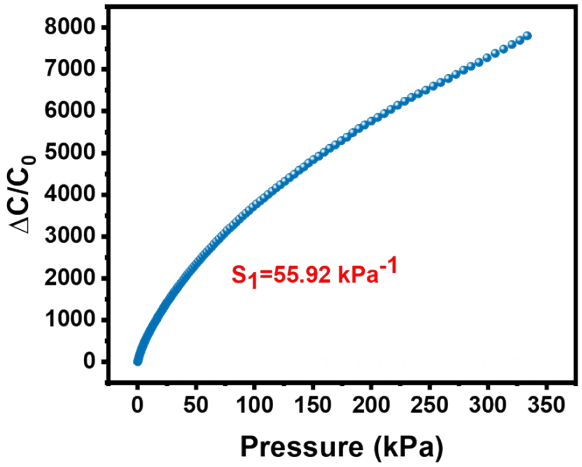


Fig. S10 Pressure–capacitance response curve of the sensor without porous separator.

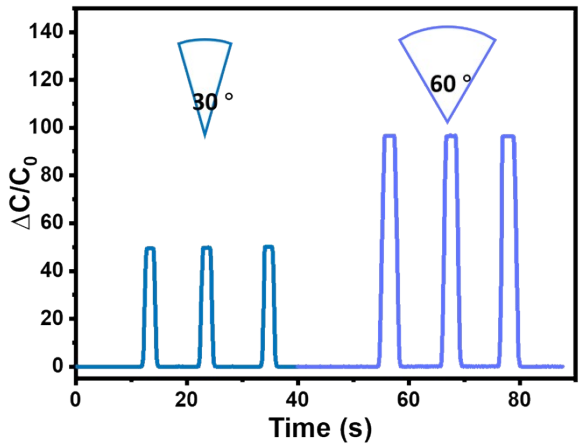


Fig. S11. Capacitance response of the IPS pressure sensor under bending at flexion angles of 30° and 60°.

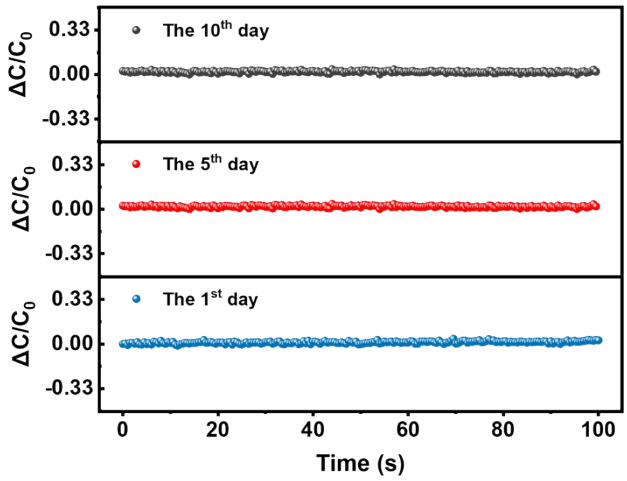


Fig. S12. The changes in sensor capacitance measured on the 1st, 5th, and 10th days under conditions of 80% relative humidity and 30°C.

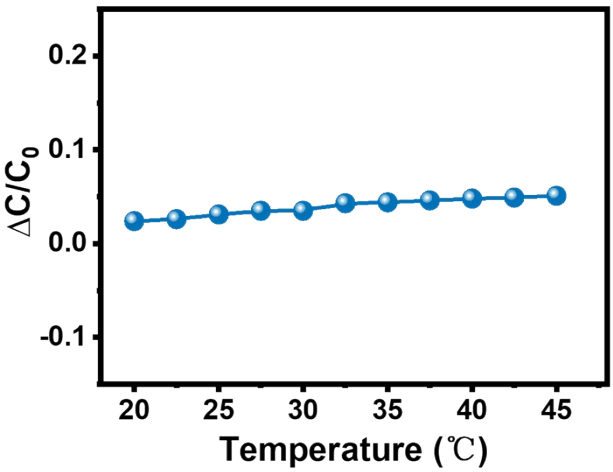


Fig. S13. Relative capacitance variation of the IPS sensor over a wide temperature range from 20 °C to 45 °C.

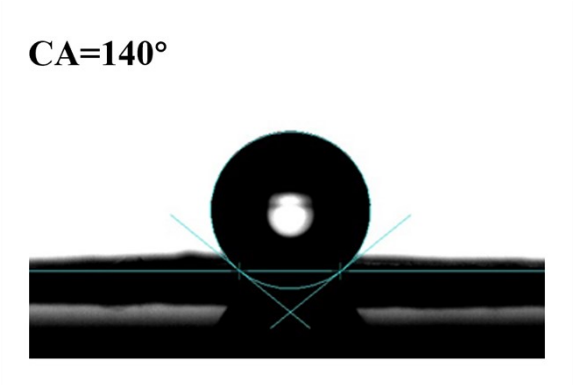


Fig. S14. Water contact angle of the sensor surface.

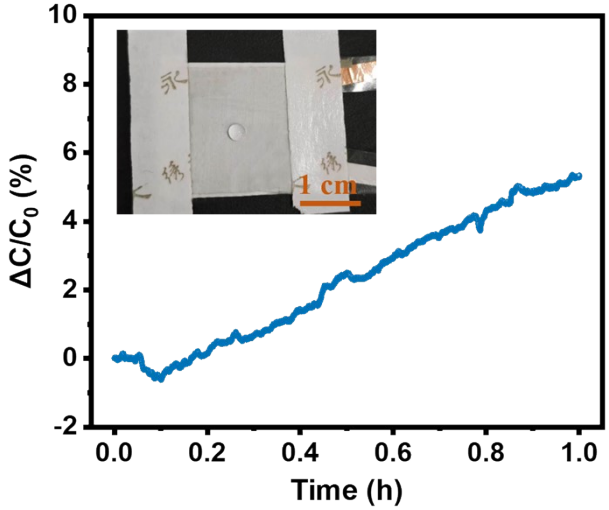


Fig. S15. Capacitance stability of the sensor under artificial sweat exposure (2 μL).

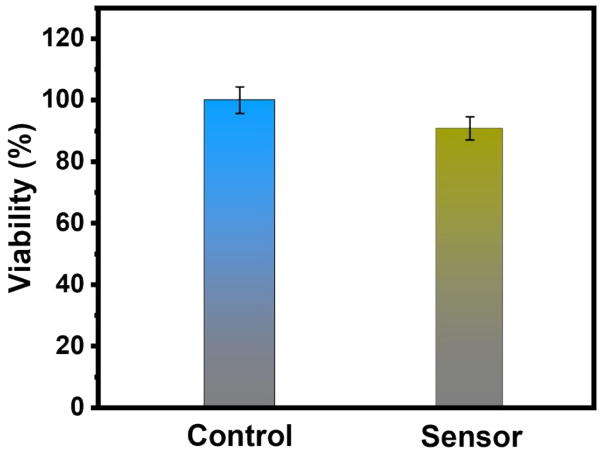


Fig. S16 Comparison of cell viability in different incubation groups.

Table S1 Effect of dielectric layer thickness on the capacitive response of the sensor, including the initial capacitance, capacitance at 200 kPa, and capacitance variation over the entire tested pressure range.

| **Thickness(μm)** | **$C_0$(pF)** | **C(pF)** | **$\Delta C/C_0$** |
|---|---|---|---|
| **57** | 128 | 799308 | 6243.6 |
| **90** | 11.3 | 71924 | 6364 |
| **126** | 13 | 64 | 3.9 |

Table S2 Comparison of the sensor with representative breathable wearable electronic textiles regarding air permeability, moisture vapor transmission rate (MVTR), sensitivity, detection limit, and pressure sensing range.

| Sample | Air permeability | MVTR | Sensitivity | Detection limit | High sensitivity pressure range | Ref. |
|---|---|---|---|---|---|---|
| MXene/AgNWs/ nonwovens | NR | NR | 14.28 $kPa^{-1}$ | 0.25 kPa | 0.25–5 kPa | [41] |
| MCSF | 91.85 mm $s^{-1}$ | 2750 g $m^{-2}$ $d^{-1}$ | 0.1891 $kPa^{-1}$ | 500 Pa | 5–30 kPa | [36] |
| CM/CA/TPU | NR | 141.7±13.16 g $m^{-2}$ $h^{-1}$ | 2.1 $kPa^{-1}$ | 0.4 kPa | 0–5 kPa | [42] |
| Cotton fabric/ PVDF-HFP/IL | NR | NR | 11.61 $kPa^{-1}$ | 2.8 Pa | 0–50 kPa | [43] |
| AFCS | 7.56 $cm^3/s$ $cm^2$ | NR | 8.31 $kPa^{-1}$ | 0.5 Pa | 0–1 kPa | [44] |
| CF p-textile | NR | NR | 17.73 $kPa^{-1}$ | 2 Pa | 0.1–30 kPa | [45] |
| BAT sensor | 448.77 mm $s^{-1}$ | 147.11 g $m^{-2}$ $h^{-1}$ | 0.33 kPa−1 | 0.25 Pa | 6–21 kPa | [46] |
| DMWES | NR | 13.99 kg $m^{-2}$ $d^{-1}$ | 548.09 $kPa^{-1}$ | 0.44 kPa | 0–6 kPa | [47] |
| TPU@PANI NM | NR | 666.95 g $m^{-2}$·$d^{-1}$ | 31.73 $kPa^{-1}$ | 1 Pa | 0–0.5 kPa | [48] |
| PEDOT/MWCNT@PU | NR | NR | 1.6 kPa−1 | 4 Pa | 8–30 kPa | [49] |
| TEM sensor | 25.6 mm $s^{-1}$ | 2051 g $m^{-2}$ $d^{-1}$ | 27.4 $kPa^{-1}$ | 2 kPa | 0–10 kPa | [50] |
| **Our work** | **12.53 mm $s^{-1}$** | **100.28g $m^{-2}$ $h^{-1}$** | **96.01±3.12 $kPa^{-1}$** | **1 Pa** | **0–47 kPa** | |